Biosensors and Bioelectronics 181 (2021) 113147

Contents lists available at ScienceDirect

Biosensors and Bioelectronics

journal homepage: http://www.elsevier.com/locate/bios

A supersensitive silicon nanowire array biosensor for quantitating tumor marker ctDNA

Dujuan Li [a,1], Huiyi Chen [a,1], Kai Fan [a,b], Vladimir Labunov [c], Serguei Lazarouk [c], Xiaojie Yue [d], Chaoran Liu [a,*], Xun Yang [e,**], Linxi Dong [a], Gaofeng Wang [a,***]

[a] Ministry of Education Engineering Research Center of Smart Microsensors and Microsystems, College of Electronics and Information, Hangzhou Dianzi University, Hangzhou, 310018, China
[b] School of Automation, Hangzhou Dianzi University, Hangzhou, 310018, China
[c] Belarusian State University of Informatics and Radioelectronics, P. Browka 6, 220013, Minsk, Belarus
[d] The Children's Hospital of Zhejiang University School of Medicine, Hangzhou, 310052, China
[e] School of Electronic and Information Engineering, China West Normal University, Nanchong, 637002, China

ARTICLE INFO

Keywords:
Silicon nanowire (SiNW) array biosensor
Circulating tumor DNA (ctDNA)
PIK3CA E542K
Field effect transistor

ABSTRACT

Cancer has become one of the major diseases threatening human health and life. Circulating tumor DNA (ctDNA) testing, as a practical liquid biopsy technique, is a promising method for cancer diagnosis, targeted therapy and prognosis. Here, for the first time, a field effect transistor (FET) biosensor based on uniformly sized high-response silicon nanowire (SiNW) array was studied for real-time, label-free, super-sensitive detection of *PIK3CA* E542K ctDNA. High-response 120-SiNWs array was fabricated on a (111) silicon-on-insulator (SOI) by the complementary metal oxide semiconductor (CMOS)-compatible microfabrication technology. To detecting ctDNA, we modified the DNA probe on the SiNWs array through silanization. The experimental results demonstrated that the as-fabricated biosensor had significant superiority in ctDNA detection, which achieved ultralow detection limit of 10 aM and had a good linearity under the ctDNA concentration range from 0.1 fM to 100 pM. This biosensor can recognize complementary target ctDNA from one/two/full-base mismatched DNA with high selectivity. Furthermore, the fabricated SiNW-array FET biosensor successfully detected target ctDNA in human serum samples, indicating a good potential in clinical applications in the future.

1. Introduction

Cancer has become one of the leading issues of death worldwide (Bray et al., 2018). Most current diagnosis methods only rely on tissue biopsy, which is an invasive test and provide only static information about the tumor (Calapre et al., 2017). To comfort the patient, a non-invasive liquid biopsy detection method was developed to achieve real-time dynamic monitoring of cancer and determine suitable therapeutic method by detecting free molecules (circulating tumor DNA (ctDNA), circulating tumor cells (CTCs), metabolites, etc). CTCs detection (Zhang et al., 2019; Miccio et al., 2020; Sun et al., 2019) has been studied for cancer screening and treatment evaluation. However, the number of CTCs in blood is very low in the early stages of cancer, some rare cells may be misdiagnosed as CTCs, resulting in false positives. Although metabolic analysis (Cao et al., 2020; Huang et al., 2020; Wan et al., 2020) can better understand the progress of the disease, the low levels of metabolites in patient samples makes it unable to meet the requirements of accurate diagnosis. ctDNA (Diaz and Bardelli., 2014) is a nucleic acid fragment released by tumor cells into the peripheral blood. Compared with CTCs, metabolites and other substances, the amount of ctDNA can effectively reflect the tumor burden in the body (Wang et al., 2015). In addition, the half-life of ctDNA in blood is short, from 2 h to one day (Zhang et al., 2018). Dynamic monitoring of ctDNA can accurately observe the chronic response of tumors, which is of great value for the prognosis of diseases and targeted therapy. Practically, E542K (G70271A in exon 9) (Cai et al., 2018; Nguyen and Sim., 2015),

* Corresponding author.
** Corresponding author.
*** Corresponding author.
E-mail addresses: liucr@hdu.edu.cn (C. Liu), yangxunjr@163.com (X. Yang), gaofeng@hdu.edu.cn (G. Wang).
[1] These authors contributed equally to this work.

https://doi.org/10.1016/j.bios.2021.113147
Received 18 January 2021; Received in revised form 27 February 2021; Accepted 3 March 2021
Available online 5 March 2021

Table 1
Sequences of capture probe DNA and target DNA.

DNAs	Sequences
ssDNA probe	5′–COOH–CCCCCCAGTGATTTTAGAGAG-3′
complementary DNA (ctDNA)	5′-CTCTCTAAAATCACT-3′
one-base mismatched DNA	5′-CTCTCTGAAATCACT-3′
two-base mismatched DNA	5′-CTCTCTGAAATGACT-3′
non-complementary DNA	5′-TACTCCGCGCTAACG-3′

as a common mutation hotspot in ctDNA of *PIK3CA*, widely exists in gastric cancer, breast cancer, lung cancer, liver cancer, colon cancer and brain cancer (Banerji et al., 2012; Cai et al., 2018; Dawson et al., 2013). Therefore, developing an efficient *PIK3CA* E542K ctDNA detection technology has great significance to tumor diagnosis, prognosis and targeted therapy.

Numerous approaches to qualitatively detecting ctDNA have been proposed, such as electrochemical impedance measurement (Sahoo et al., 2013), localized surface plasmon resonance (LSPR) technology (Nguyen and Sim., 2015), droplet digital PCR (ddPCR) (Kang et al., 2016), amplification refractory mutation system (ARMS) (Feng et al., 2018), and DNA hydrogels (Mao et al., 2019). However, these reported methods still have some limitations: 1) Effective processing and accurate readout of DNA recognition signals are challenging. 2) Achieving high sensitivity requires expensive, large scale equipment and multistep processes, which limits their large-scale applications. Therefore, it is urgent to develop an ultrasensitive, label-free, low-cost, and portable ctDNA detection method.

To addressing the limitations, nanomaterials (HelmyAbdou et al., 2019; Jandas et al., 2020; Li et al., 2015; Mu et al., 2016; Salimi et al., 2013; Zhang et al., 2017) with superior conductive properties open up new strategies. Silicon nanowire (SiNW), as an excellent candidate material, has been widely studied for applying in biomedicine (Gao et al., 2020; Tsai et al., 2011; Wu et al., 2018), industrial production (Liu et al., 2017; Thiyagu et al., 2011; Tian et al., 2007) and microfluidics (Liu et al., 2018) due to its large surface-to-volume ratio and excellent biocompatibility. Additionally, it has good holes or electrons transfer capabilities in detection because of the accumulation of charges in SiNWs, which can sensitively perceive small changes in the surface electrostatic field environment (Gao et al., 2011, 2012). SiNW-based field effect transistor (SiNW-FET) (Li et al., 2016; Wu et al., 2018) has shown a great potential for biological detection, especially in DNA (Lu et al., 2016).

The performance of the SiNW-FET sensor is mostly determined by the number of SiNWs (Gong et al., 2015). In most of the previously reported SiNW sensing systems (Li et al., 2016), the number of SiNW in the array is usually only a few or a dozen, which has a picoampere detecting electrical signals requiring precise instrument. In our previous research, we proposed a SiNW manufacturing technology (Yang et al., 2018) compatible with complementary metal oxide semiconductor (CMOS) technology, which can precisely control the dimension of SiNWs and achieve mass manufacturing. Compared with the previously reported SiNW sensor (Nuzaihan et al., 2016), the integrated SiNW array sensor showed low cost, higher signal-to-noise ratio, and higher sensitivity with microampere current signal (Yang et al., 2019). This SiNW-FET sensor has successfully applied in vapor analytes (Gao et al., 2017b) and liquid tumor markers detection (Yang et al., 2019).

Given the excellent performance, we firstly present a wafer-level,

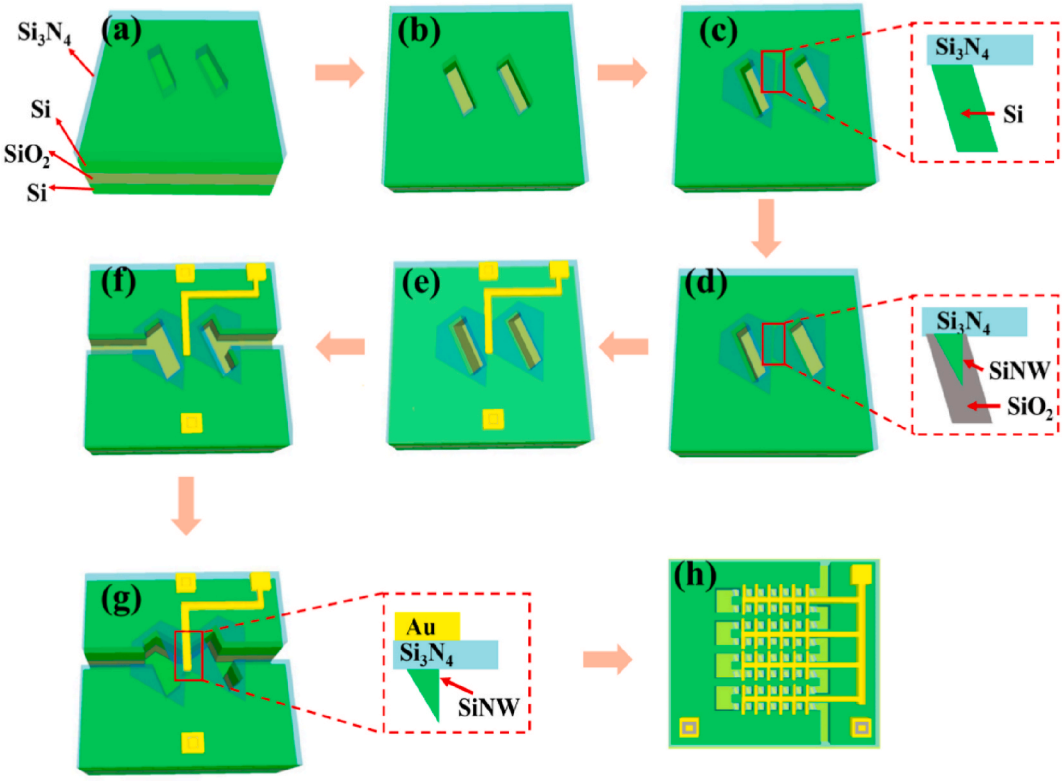

Fig. 1. The fabrication processes of SiNW array sensor on (111) SOI wafer. (a) Silicon nitride was etched to form two adjacent rectangular cavities, then deep reaction ion etching to form etched cavities (b). By anisotropic wet-etching, a silicon wall was formed between the adjacent etched cavities (c), the right part was a sectional drawing. After Self-limiting oxidation, a SiNW was generated on the top center of walls (d), the right part was a sectional drawing. Source electrode, drain electrode and a top-grid electrode were fabricated (e), and the trench was performed to isolate source electrodes and drain electrodes (f). Finally, the single SiNW-FET formed after removing the silica wall (g), the right part was a sectional drawing. Rectangle box was a local amplification sectional drawing of SiNW, where the arrow mark was the SiNW. In this way, the SiNW-array FET were integrated on a (111) SOI wafer (h). (For interpretation of the references to colour in this figure legend, the reader is referred to the Web version of this article.)

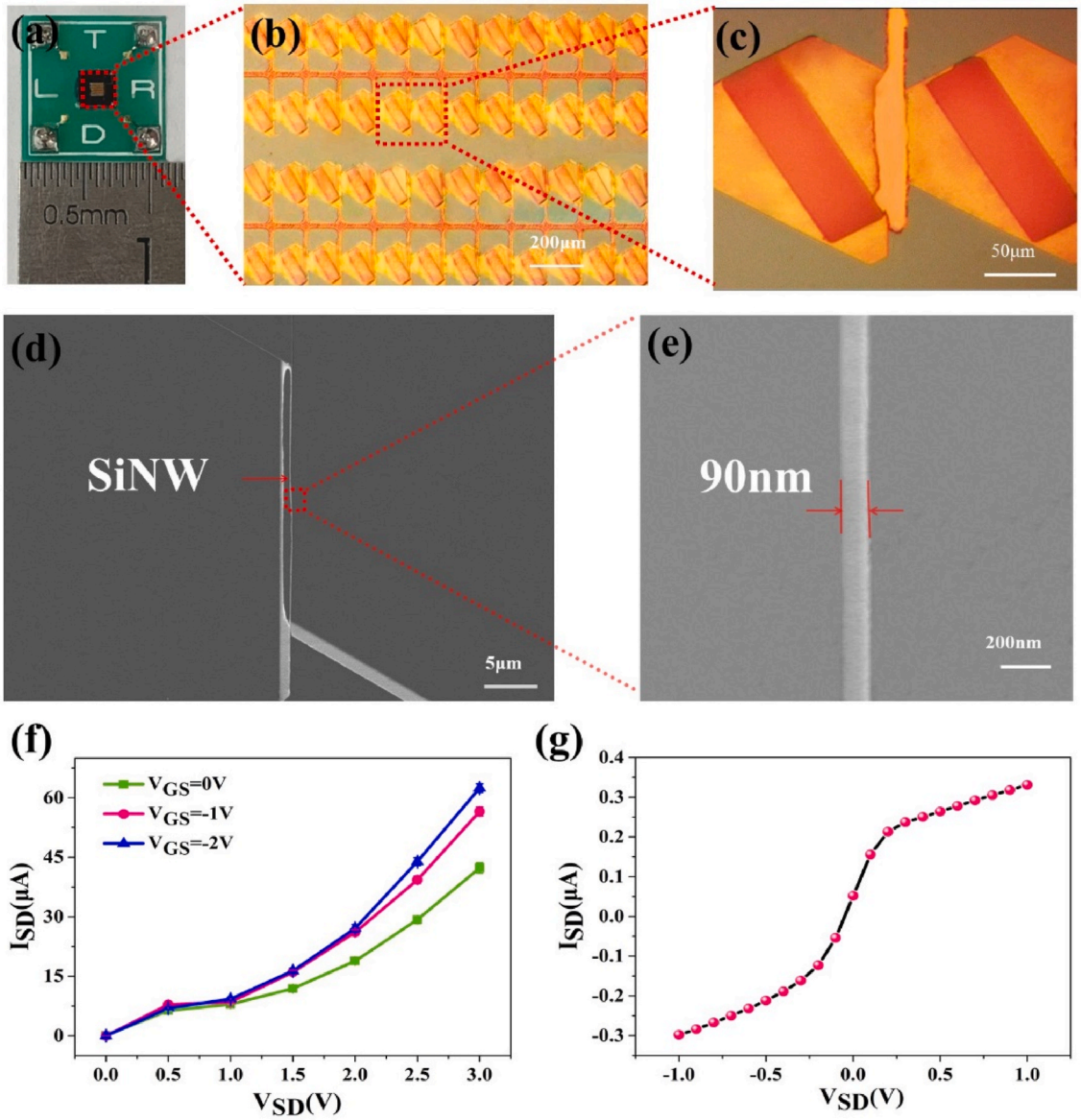

Fig. 2. Photograph of packaged SiNW-array FET devices (a), and optical microscope images of partially enlarged silicon wall arrays (b) and local amplification (c). The SEM image of a single SiNW (d) and local amplification (e). (f) I–V characteristics of the SiNW-array FET sensor in air. I_{SD}/V_{SD} curve for varying V_{GS} (0 to −2 V, ΔV = −1 V). (g) I–V characteristics of the SiNW-array FET sensor in PBS solution at V_{GS} = 0 V. (For interpretation of the references to colour in this figure legend, the reader is referred to the Web version of this article.)

highly controlled p-type SiNW-array FET biosensor for quantitating tumor marker *PIK3CA* E542K ctDNA in this paper. The SiNW arrays were fabricated on a commercial (111) silicon-on-insulator (SOI) wafer using a novel low-cost CMOS technology. After a series of surface modification processes, specific single-stranded DNA (ssDNA) probes were assembled on the surface of SiNWs to identify and detect ctDNA. The SiNW array biosensor showed an ultralow limit of detection as low as 10 aM and high specificity for the recognition of single-nucleotide polymorphism (SNP). The human serum samples were also studied using the fabricated SiNW-array FET biosensor.

2. Materials and methods

2.1. Materials and reagents

We purchased experimental reagents such as N-hydroxysuccinimide (NHS), 1-ethyl-3-(3-dimethylaminopropyl) carbodiimide (EDC), phosphate buffered saline (1 × PBS, 137 mM NaCl, 2.7 mM KCl, and 10 mM phosphate, pH 7.2–7.4), and absolute ethanol from Shanghai Macklin Biochemical Co., Ltd (China), and 3-aminopropyltriethoxysilane (APTES) obtained from Sigma-Aldrich (USA).

The oligonucleotides of the ctDNA were synthesized from Shanghai Sangon Biotech Co., Ltd (China). The sequences of probe DNA and target DNAs were listed in Table 1. The one/two-base mismatch DNAs contained the E542K mutation site (see from Supporting Information S1).

2.2. The fabrication of SiNW array sensor

The wafer-level and highly controllable SiNW array FET was fabricated with a top-down microfabrication process (Fig. 1) based on our previous research basis (Yang et al., 2018). SiNW array with inverted triangular structure was obtained by precisely controlling wet etching parameters (e.g., wet etching time, wet etching rate, and dry etching depth). Meanwhile, the top-grid electrode was designed to protect the SiNW from breakage.

In order to quickly and accurately identify target ctDNA, a

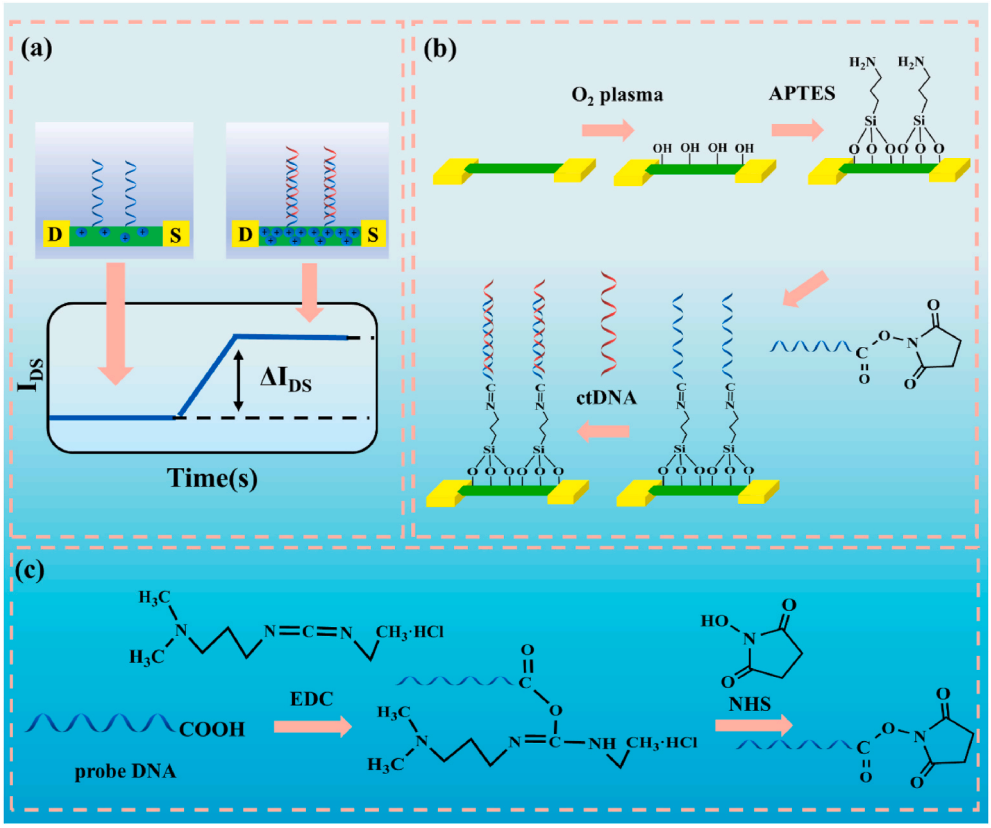

Fig. 3. (a) Working principle of the SiNW-array FET biosensor, (b) the stepwise process of fabrication and detection of SiNW-array FET biosensor for tumor marker ctDNA, (c) schematic diagram of carboxyl groups activation by EDC/NHS.

polydimethylsiloxane (PDMS) microcavity structure was designed on the top of the sensing area, which directs the solution to the SiNWs. The microfluidic structure effectively reduced the interference caused by the external environment and achieved the rapid transportation of ctDNA molecules.

2.3. Surface modification and hybridization

The ssDNA probe was assembled onto the surface of the SiNW array to identify ctDNA via a series of specific modification approaches (Fig. 3 (b)). The surface of the entire sensor was first treated with oxygen (O_2) plasma for 5 min and then immersed in 2% v/v APTES in 99.5% ethanol at room temperature overnight. Prior to immobilizing the probe DNA, the carboxyl group at terminal of probe DNA was activated by a mixture of NHS and EDC (1:1) for 30 min. Subsequently, ssDNA probe solution (0.5 μM) in PBS was pipetted into PDMS well and then incubated for 2 h at room temperature. Superfluous of ssDNA probe was then removed by PBS cleaning. After the immobilization step, a recognition function layer (ssDNA/SiNW-array FET) was formed on the surface of the sensor. This meant that a specific biosensor has been ready for target ctDNA detection. Finally, *PIK3CA* E542K ctDNA solution was pipetted into the PDMS well to hybridize with probe DNA.

2.4. Characterization of SiNW-array FET biosensors

The specificity, sensitivity and stability of SiNW-array FET biosensor were electrically characterized by using a Keithley 2450 sourcemeter (Keithley Instruments Inc., Cleveland, OH). A metalloscope (Ruihong, Type HJ1) and scanning electron microscopy (SEM) (JEOL JSM6460LA) were applied to verify the quality of SiNWs. The source-drain voltage was swept from −1 V to 1 V to characterize the silanization, DNA immobilization, and hybridization. For the measurements, we applied V_{SD} = 1 V, V_{GS} = 0 V to the SiNW-array FET biosensor. All the experiments were conducted in a dark environment.

2.5. Preparation of human serum samples

Blood samples were collected from ten healthy volunteers and five of them randomly chosen for the experiments. The supernatant was collected after blood clotting. Serum samples were separated by centrifugation of the supernatant at 3000 rpm for 15 min. 1:10 dilution of serum samples were analyzed alone or spiked with ctDNA to final concentrations of 100 fM, 1 pM, 10 pM, 100 pM, 1 nM.

This study was approved by the local research ethics committee (No. 2019-IRB-088, The Children's Hospital of Zhejiang University School of Medicine, Hangzhou, China). All subjects gave informed consent. Subjects confidentiality was preserved.

3. Results and discussion

3.1. Fabrication and transfer characteristics of SiNW-array FET sensor

The high responsive p-type SiNW array FET were fabricated through CMOS-compatible microfabrication processes. The packaged SiNW-array FET devices, and partially enlarged silicon wall arrays were shown in Fig. 2(a ~ c). The 120-SiNWs with inverted-triangle structure cross-section were fixed between the source and drain electrode in the form of 15 × 8 array to serve as the sensing region. The cross-sectional dimensions of SiNWs were approximately 90 nm (Fig. 2(d) and (e)) with a deviation less than ± 20 nm. The high uniform size of SiNWs can further improve the sensitivity of the biosensor (Yang et al., 2018).

The transmission characteristics of the SiNW-array FET sensor were measured by Keithley 2450. The results were shown in Fig. 2(f) and (g). The SiNW-array FET sensor exhibited typical depletion mode nanowire

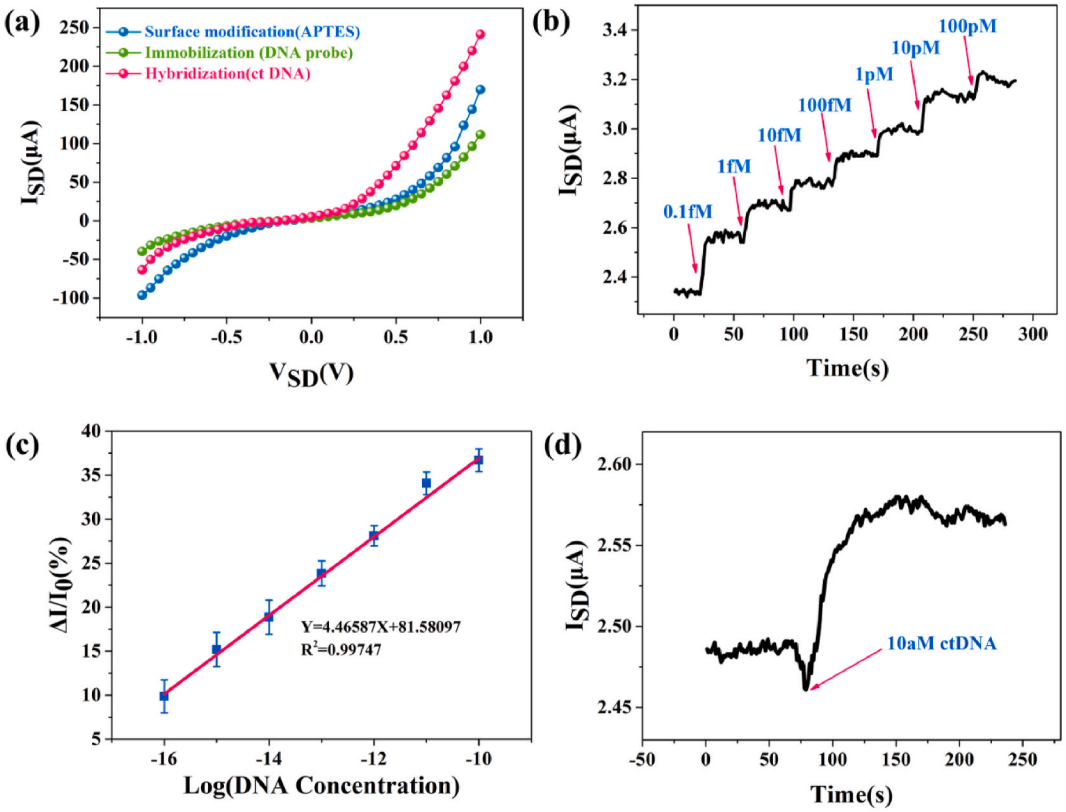

Fig. 4. (a) I–V characteristics of the same SiNW-array FET sensor at different stage. (b) The real-time response of SiNW-array FET biosensor for different concentrations of ctDNA (from 0.1 fM to 100pM). Red arrows indicate the points of injections. (c) Calibration curve of the normalized current change for a series concentration of ctDNA (0.1 fM, 1 fM, 10 fM, 100 fM, 1 pM, 10 pM, 100 pM). (d) Real-time current response of SiNW-array FET biosensor for 10 aM ctDNA (V_{SD} = 1 V). (For interpretation of the references to colour in this figure legend, the reader is referred to the Web version of this article.)

current-voltage (I–V) transmission characteristics under both gas and liquid phase. Fig. 2(f) showed I–V characteristics of the SiNW-array FET sensor measured under the V_{SD} from 0 to 3 V (step: 0.5 V), while the V*GS* from 0 to −2 V (step: 1 V) in the air. Fig. 2(g) showed the I_{SD}-V_{SD} characteristics in the liquid with fixed gate voltage (0 V) and source-drain voltage sweeping from −1 to 1 V. The above results showed that the gate of the SiNW-array FET sensor had a good regulating effect on the source/drain current and exhibited superior Schottky contact in liquid phase. The SiNW-array FET device was available for biosensor fabrication and detection.

3.2. Working principle of the SiNW-array FET biosensor

Due to the high surface-to-volume ratio, SiNWs are ultra-sensitive to the variation of the external electric field environment. Therefore, each SiNW can be used as a ctDNA sensing unit (Gao et al., 2017a). The surface of SiNWs was firstly silanized to generate a self-assembled monolayer of terminal amino groups, and then modified with bio-probes to form "molecular gate" via capturing target ctDNA (Nuzaihan et al., 2016). Lots of hole carriers will be accumulated rapidly in the SiNWs as the bio-probes capture the ctDNA with negatively charge, which increases the I_{SD} (Fig. 3(a)).

This molecular gate control effect is consistent with the semiconductor nanowire devices as previously reported (Nuzaihan et al., 2016). The DNA hybridization is recognized by the SiNW-array FET biosensor accompanying electrical signals output, which can dynamically monitor the target ctDNA.

3.3. Transfer characteristics of immobilization and hybridization

For a biosensor, functionalizing the sensing surface through specific molecules determines the sensitivity and stability of the sensor. Therefore, the critical step is the SiNWs surface pretreatment by O_2 plasma (Rahman et al., 2016) (70 W, 5 min) to remove the surficial inherent impurities. Meanwhile, rich terminal hydroxyl groups (-OH) were also generated on the surface of SiNWs, which improving the hydrophilic characteristics of the SiNW surface (Supporting Information, S2). Then, the SiNW-array FET chip was silanized by 2% v/v APTES to form the APTES/SiNW-array FET (Fig. 3(b)).

The electrical characteristics of SiNW-array FET biosensor was qualitatively analyzed by Keithley 2450. The I–V characteristics in Fig. 4 (a) indicated the current response in silanization (APTES), immobilization (ssDNA probe), and hybridization (double-stranded DNA). The APTES solution is alkaline because the nitrogen atom of the APTES amino group attracts H^+ in the solution contributing to form NH_3^+ and OH^-. Si–OH tends to deprotonate and form negative charges ($Si–O^-$) in this alkaline solution, which is equivalent to applying a negative electric field outside the sensor.

Due to NHS and EDC, the terminal carboxyl group (-COOH) of the probe was activated (Fig. 3(c)), promoting the condensation reaction with amino groups on the sensor surface. In the formed peptide bond (CO═NH), each atom was covalently bonded without unshared electron pairs, reducing the ability to attract H^+. The decrease in the alkalinity of the solution reduces the negative charge on the surface of the sensor, which decreases the current in the SiNW (Fig. 4(a)). The sensing mechanism was consistent with the principle of pH detection by SiNW array FET (Supporting Information, S3). Therefore, the current after probe modification decreased compared with the silanization.

The hybridization of target ctDNA and probe DNA increase the current significantly by promoting positive current movement (Fig. 4 (a)). ctDNA with negative charges forms a larger negative electric field on the surface of SiNW and increases the positive charges carrier density

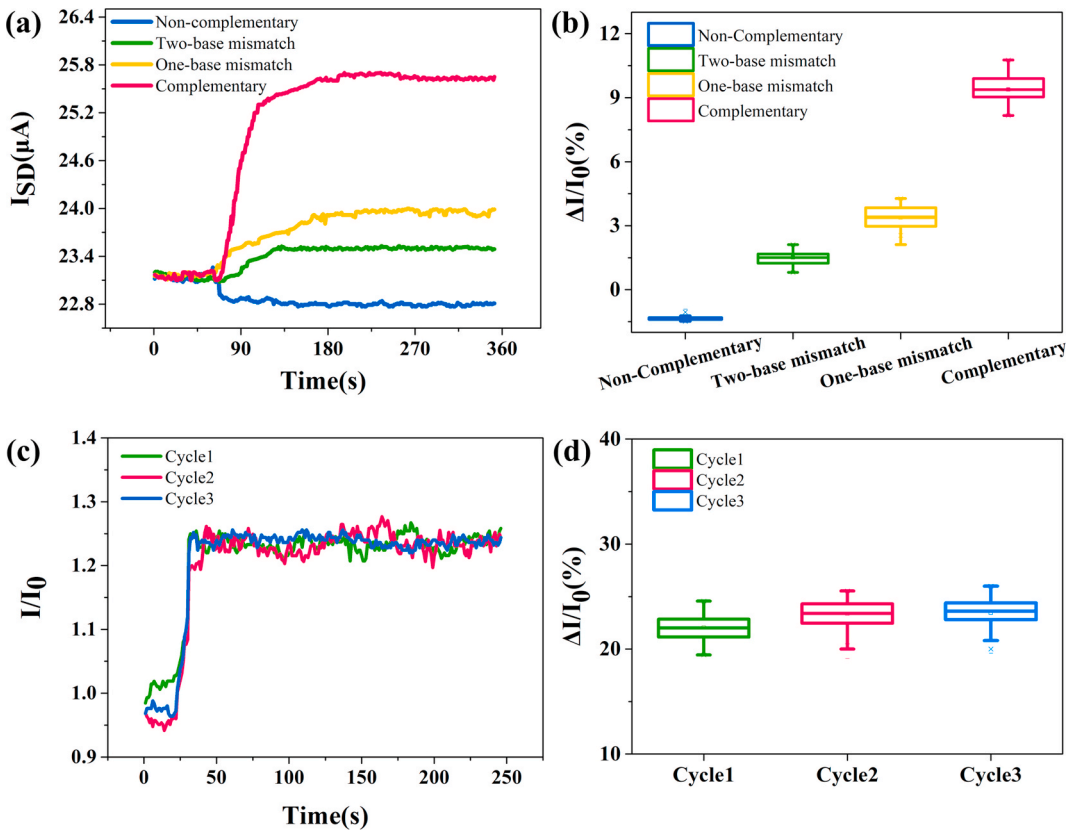

Fig. 5. Evaluation of the specificity (a, b), repeatability (c) and reproducibility (d) of the SiNW-array FET biosensor. (a)The current response of the different hybridization at the same sample concentration (100 pM). (b) The normalized current change plots of non-complementary, two-base mismatched, one-base mismatched, and complementary target DNAs. The normalized current changes of 100 fM target ctDNA at the same SiNW-array FET biosensor (c) and different SiNW-array FET biosensors (d). Error bars indicate the standard deviation (n = 3).

inside the SiNWs, which increases the current. The results was consistent with the previously reported mechanism of semiconductor nanowire biosensors (Li et al., 2014; Shen et al., 2014).

3.4. Detection and sensitivity of SiNW-array FET biosensor

Different concentration of target ctDNA was monitored by the SiNW-array FET biosensor in real time in the range of 10 aM–100 pM. Specifically, PBS buffer was introduced into the sensor surface to establish the baseline current I_0 after immobilizing ssDNA, and then adding a known concentration of ctDNA solution. In p-type SiNW, the majority charges carriers are the holes. A large amount of charge carriers (holes) would accumulate inside the SiNWs when more negatively charged ctDNA was specifically captured by the probe on the surface of SiNWs, resulting in a larger increase in I_{SD}. As shown in Fig. 4(b), the source-drain current increased stepwise with the increasing ctDNA concentration. Obvious current changes were observed when a series of 0.1 fM, 1 fM, 10 fM, 100 fM, 1 pM, 10 pM, 100 pM complementary target ctDNA were introduced to hybridize with the probe-functionalized SiNWs. The current change rate was ~9.86%, ~15.19%, ~18.86%, ~23.84%, ~28.12%, ~34.07%, ~36.69%, respectively (Fig. 4(c)) with the increasing concentration.

The results indicated that the relative current change had a highly dependent linear relationship with logarithm of target ctDNA concentration, especially for the concentration ranging from 0.1 fM to 100 pM. Fig. 4(c) showed a calibration curve of the normalized current change versus target ctDNA concentration (0.1 fM, 1 fM, 10 fM, 100 fM, 1 pM, 10 pM, 100 pM). The equation of linear regression after calibration fitting was $Y = 4.46587X + 81.58097$ with the $R^2 = 0.99747$, where X was the mean of the logarithm of target ctDNA concentration.

The relationship between sensitivity and SiNW size can be illustrated by the following equation (Yang et al., 2018, 2019):

$$sensitivity = \frac{\Delta I}{I_0} = \frac{(I - I_0)}{I_0} = \frac{K}{\overline{\omega}} - \frac{K}{\overline{\omega}^2}(\omega - \overline{\omega}) \quad (1)$$

where K is a constant, ω is the dimension of SiNW, $\overline{\omega}$ is the average dimension of SiNWs, I_0 and I are the current response before and after the hybridization of ctDNA. It can be seen from equation (1) that the sensitivity of SiNW is highly correlated with the dimension of the nanowire. Obviously, the SiNW with the same dimension can produce the same signal. Compared with a single SiNW, 120 SiNWs with high consistency of dimensions make the signal superimpose, resulting in the much stronger response signal and higher signal-to-noise ratio.

The limit of detection (LOD) is calculated using $Y_{LOD} = Y_{blank} + 3\sigma$, where Y_{blank} is the response of blank measurement and σ is standard deviation of blank measurement (Rahman et al., 2016; Yusoh et al., 2019). The blank response of SiNW array biosensor detection was 2.48 × 10^{-6} A, and the standard deviation was 1.21 × 10^{-8} A, so the threshold response current was calculated to be 2.52 × 10^{-6} A. As shown in Fig. 4(d), the stable current response of target ctDNA (10 aM) was 2.56 × 10^{-6} A, which was larger than the threshold response. So, the SiNW-array FET biosensor showed an ultra-high sensitivity, with a detection limit of 10 aM. The experimental results proved that the SiNW array biosensor with uniform size had significant advantages in DNA detection sensitivity.

3.5. Specificity, repeatability and reproducibility of SiNW array biosensor

3.5.1. Specificity

To verify the specific recognition of target ctDNA by the SiNW-array

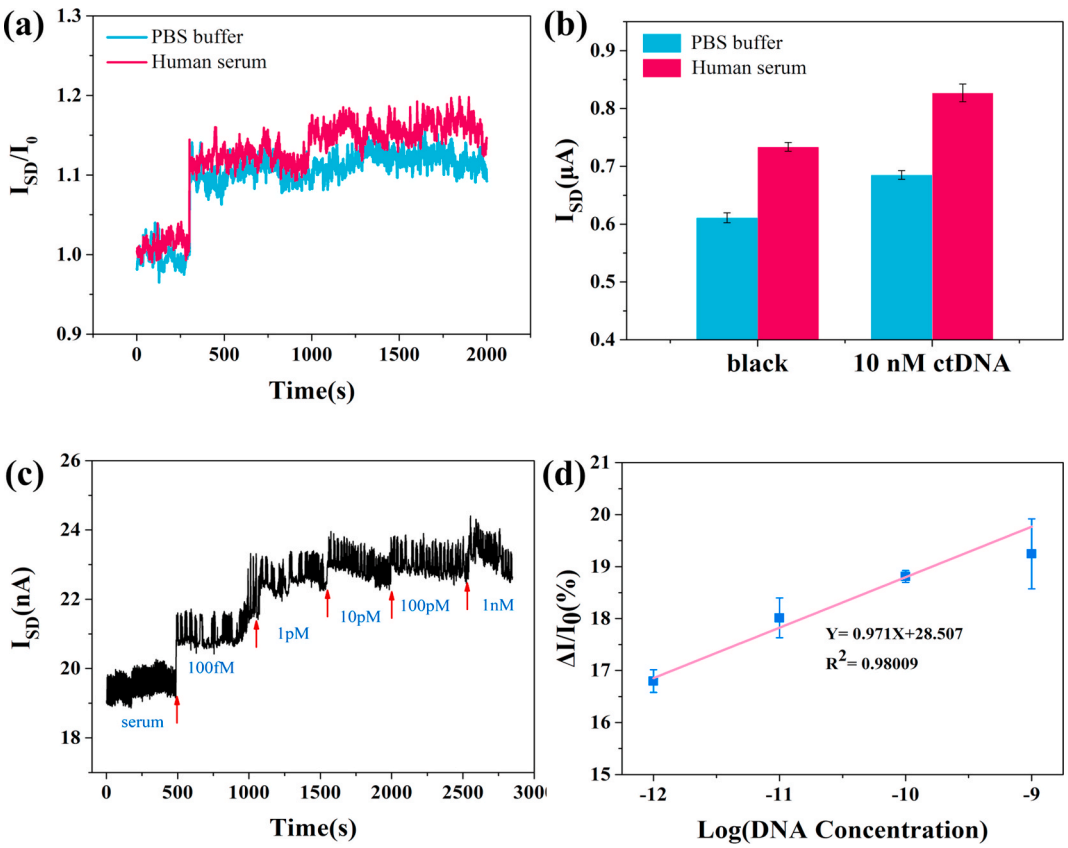

Fig. 6. Evaluation of SiNW-array FET biosensor using human serum. (a) Real-time response of SiNW-array FET biosensor to 10 nM ctDNA diluted with (red area) or without (blue area) human serum. (b) Column plot of the relative current change of SiNW-array FET biosensor for 10 nM ctDNA diluted with (red area) or without (blue area) human serum. (c) Real-time response of SiNW-array FET biosensor for different concentrations of target ctDNA (100 fM, 1 pM, 10 pM, 100 pM, 1 nM). (d) Relative current change of SiNW-array FET biosensor as a function of the logarithm of target ctDNA concentration. (For interpretation of the references to colour in this figure legend, the reader is referred to the Web version of this article.)

FET biosensor, the same concentration (100 pM) of one-base mismatched, two-base mismatched and non-complementary DNA were introduced into SiNW-array FET, respectively. ctDNA is fragmented to an average length of 50–250 base pairs (Cai et al., 2018) and E542K is a common mutation hotspot in ctDNA of *PIK3CA,* which is often mutated from A to G. The one-base mismatch DNA was the E542K mutation sequence, and the two-base mismatch DNA contained the E542K mutation site (details in Supporting Information, S1).

Fig. 5(a) indicated that non-complementary DNA (100 pM) (~-1.34%) and two-base mismatched DNA (100 pM) (1.50%) did not cause significant changes in current. The relative current change rate was ~3.37% when one-base mismatched DNA was introduced to the SiNWs surface. Obviously, as shown in Fig. 5(b), the current change rate was about 10.54% while hybridization of complementary DNA, which was three times the change of the current for one-base mismatched DNA. The tests results demonstrated the good specificity for SNP detection, allowing the distinction between one, two-mismatched, non-complementary and complementary DNA (Gao et al., 2011; Nuzaihan et al., 2016). This is of great significance for the screening of related cancers. Specificity was also confirmed at different target concentrations (Supporting Information, S4).

3.5.2. *Repeatability and reproducibility*

O_2 plasma treatment can remove a large amount of impurities on the surface (Zhang et al., 2020) except for being an effective strategy to increase surface hydrophilicity (Rahman et al., 2016). Therefore, the same SiNW-array FET sensor was treated with O_2 plasma (70 W) for 5 min and then refabricated to detect 100 fM target DNA. The data was normalized by calculating I_{SD}/I_0 and plotted on the same axis to effectively compare the relative changes of the SiNW current detected by 100 fM ctDNA after 3 refabrications. The biosensor exhibited excellent repeatability, which has a consistent response in three cycles (Fig. 5(c)).

The reproducibility was also studied using different devices. The repeatable performance results of the sensor were shown in Fig. 5(d). After 3 cycles, the relative current changes of 100 fM target DNA still showed a high consistency, 22.00%, 23.59%, 23.51% respectively, showing a good reproducibility.

3.6. *Simulation analysis of human serum samples*

To further evaluate the clinical application potentiality of our SiNW array biosensor, serum samples from healthy people spiked with different concentrations of target ctDNA were analyzed. High concentration (10 nM ctDNA) serum samples were firstly tested by the SiNW-array FET biosensor. In Fig. 6(a), a consistent current change was observed in PBS solution and serum samples. However, the detection background signal was increased (Fig. 6(b)) due to the relatively complex composition of the serum, including various plasma proteins, peptides, fats, carbohydrates, growth factors, and other substances. Though the detection background signal of human serum was significantly higher than that in PBS solution, the relative current change in serum and PBS was 12.7% and 12.1%, respectively, which demonstrated the feasibility of real sample detection using the SiNW-array FET biosensor.

Furthermore, the SiNW-array FET biosensor was also used to detect different concentrations of ctDNA in serum. Human serum samples were spiked with ctDNA to final concentrations of 100 fM, 1 pM, 10 pM, 100 pM, 1 nM (Fig. 6(c)). In Fig. 6(d), a linear relationship was observed

between source-drain current and the logarithmic value of the ctDNA concentration in the range of 1 pM–1 nM, with the $R^2 = 0.98009$. The signal threshold was calculated according to the same method in section 3.4, and the detection limit was 10 fM for the SiNW-array FET biosensor in human serum sample. The LOD had a huge rise for target ctDNA in human serum, in contrast to in PBS (Fig. 4), which might be owing to the interferences of complex composition such as various plasma proteins. Therefore, in the further study, it is necessary to improve the enrichment of ctDNA to achieve the high sensitivity detection of ctDNA in complex samples.

4. Conclusion

A novel quantificational detecting *PIK3CA* E542K ctDNA method was achieved by a FET biosensor based on uniformly sized high-response SiNW array, which has the advantages of real-time, label-free, supersensitive detection. The 120 SiNWs were modified with the probe DNA through silanization and acted as a molecular gate for recognizing the target ctDNA. The experimental results demonstrated that the asfabricated biosensor had significant superiority in ctDNA detection, which achieved ultralow detection limit of 10 aM and a good linearity under the ctDNA concentration range from 0.1 fM to 100 pM. The study also demonstrated that the fabricated SiNW-array FET biosensor had good specificity, repeatability and reproducibility. Significantly, the human serum samples tests showed that the SiNW-array FET biosensor could distinguish target ctDNA in complex samples and had a good potential in clinical application in the future.

CRediT authorship contribution statement

Dujuan Li: Conceptualization, Methodology, Writing - review & editing. **Huiyi Chen:** Investigation, Validation, Writing – original draft. **Kai Fan:** Data curation. **Vladimir Labunov:** Funding acquisition. **Serguei Lazarouk:** Funding acquisition. **Xiaojie Yue:** Resources. **Chaoran Liu:** Writing - review & editing, Funding acquisition. **Xun Yang:** Resources, Writing - review & editing. **Linxi Dong:** Resources. **Gaofeng Wang:** Supervision, Funding acquisition.

Declaration of competing interest

The authors declare that they have no known competing financial interests or personal relationships that could have appeared to influence the work reported in this paper.

Acknowledgements

We appreciate the financial support from the National Key R&D Program Grant (NO. 2018YFE0120000) and the National Natural Science Foundation of China (No. 31201367, 61804038).

Appendix A. Supplementary data

Supplementary data to this article can be found online at https://doi.org/10.1016/j.bios.2021.113147.

References

Banerji, S., Cibulskis, K., Rangel-Escareno, C., Brown, K.K., Carter, S.L., Frederick, A.M., Lawrence, M.S., Sivachenko, A.Y., Sougnez, C., Zou, L., Cortes, M.L., Fernandez-Lopez, J.C., Peng, S., Ardlie, K.G., Auclair, D., Bautista-Pina, V., Duke, F., Francis, J., Jung, J., Maffuz-Aziz, A., Onofrio, R.C., Parkin, M., Pho, N.H., Quintanar-Jurado, V., Ramos, A.H., Rebollar-Vega, R., Rodriguez-Cuevas, S., Romero-Cordoba, S.L., Schumacher, S.E., Stransky, N., Thompson, K.M., Uribe-Figueroa, L., Baselga, J., Beroukhim, R., Polyak, K., Sgroi, D.C., Richardson, A.L., Jimenez-Sanchez, G., Lander, E.S., Gabriel, S.B., Garraway, L.A., Golub, T.R., Melendez-Zajgla, J., Toker, A., Getz, G., Hidalgo-Miranda, A., Meyerson, M., 2012. Nature 486, 405–409.
Bray, F., Ferlay, J., Soerjomataram, I., Siegel, R.L., Torre, L.A., Jemal, A., 2018. CA A Cancer J. Clin. 68 (6), 394–424.
Cai, C., Guo, Z., Cao, Y., Zhang, W., Chen, Y., 2018. Nanotheranostics 2 (1), 12–20.
Calapre, L., Warburton, L., Millward, M., Ziman, M., Gray, E.S., 2017. Canc. Lett. 404, 62–69.
Cao, J., Shi, X., Gurav, D.D., Huang, L., Su, H., Li, K., Niu, J., Zhang, M., Wang, Q., Jiang, M., Qian, K., 2020. Adv. Mater. 32 (23), 2000906.
Dawson, S.-J., Tsui, D.W.Y., Murtaza, M., Biggs, H., Rueda, O.M., Chin, S.-F., Dunning, M.J., Gale, D., Forshew, T., Mahler-Araujo, B., Rajan, S., Humphray, S., Becq, J., Halsall, D., Wallis, M., Bentley, D., Caldas, C., Rosenfeld, N., 2013. N. Engl. J. Med. 368 (13), 1199–1209.
Diaz, L.A., Bardelli, A., 2014. J. Clin. Oncol. 32 (6), 579–586.
Feng, W.N., Gu, W.Q., Zhao, N., Pan, Y.M., Luo, W., Zhang, H., Liang, J.M., Yang, J., Deng, Y.M., 2018. Transl Oncol 11 (2), 542–545.
Gao, A., Lu, N., Dai, P., Li, T., Pei, H., Gao, X., Gong, Y., Wang, Y., Fan, C., 2011. Nano Lett. 11 (9), 3974–3978.
Gao, A., Lu, N., Wang, Y., Dai, P., Li, T., Gao, X., Wang, Y., Fan, C., 2012. Nano Lett. 12 (10), 5262–5268.
Gao, A., Wang, Y., Zhang, D., He, Y., Zhang, L., Liu, Y., Wang, Y., Song, H., Li, T., 2020. Sensor. Actuator. B Chem. 309, 127762.
Gao, A., Yang, X., Tong, J., Zhou, L., Wang, Y., Zhao, J., Mao, H., Li, T., 2017. Biosens. Bioelectron. 91, 482–488.
Gao, A.R., Wang, Y., Yang, X., Wang, Y.L., Li, T., 2017b. IEEE Sensor, pp. 1–3.
Gong, X., Zhao, R., Yu, X., 2015. Transducers-18th. Int. Conf. Solid-State Sens 1537–1540.
HelmyAbdou, K.A., Ahmed, R.R., Ibrahim, M.A., Abdel-Gawad, D.R.I., 2019. Environ. Sci. Pollut. Res. Int. 26 (35), 36063–36072.
Huang, L., Wang, L., Hu, X., Chen, S., Tao, Y., Su, H., Yang, J., Xu, W., Vedarethinam, V., Wu, S., Liu, B., Wan, X., Lou, J., Wang, Q., Qian, K., 2020. Nat. Commun. 11 (1), 3556.
Jandas, P.J., Luo, J.T., Prabakaran, K., Chen, F., Fu, Y.Q., 2020. Mater. Chem. Phys. 246, 122800.
Kang, Q., Henry, N.L., Paoletti, C., Jiang, H., Vats, P., Chinnaiyan, A.M., Hayes, D.F., Merajver, S.D., Rae, J.M., Tewari, M., 2016. Clin. Biochem. 49 (18), 1354–1360.
Li, B.R., Chen, C.C., Kumar, U.R., Chen, Y.T., 2014. Analyst 139 (7), 1589–1608.
Li, J., He, G., Ueno, H., Jia, C., Noji, H., Qi, C., Guo, X., 2016. Nanoscale 8 (36), 16172–16176.
Li, L., Zhang, L., Yu, J., Ge, S., Song, X., 2015. Biosens. Bioelectron. 71, 108–114.
Liu, C., Sun, J., Li, J., Xiang, C., Che, L., Wang, Z., Zhou, X., 2017. Sci. Rep. 7 (1), 7552.
Liu, C., Sun, J., Zhuang, Y., Wei, J., Li, J., Dong, L., Yan, D., Hu, A., Zhou, X., Wang, Z., 2018. Nanoscale 10 (48), 23164–23169.
Lu, N., Gao, A., Zhou, H., Wang, Y., Yang, X., Wang, Y., Li, T., 2016. Chin. J. Chem. 34 (3), 308–316.
Mao, X., Pan, S., Zhou, D., He, X., Zhang, Y., 2019. Sensor. Actuator. B Chem. 285, 385–390.
Miccio, L., Cimmino, F., Kurelac, I., Villone, M.M., Bianco, V., Memmolo, P., Merola, F., Mugnano, M., Capasso, M., Iolascon, A., Maffettone, P.L., Ferraro, P., 2020. View 1 (3), 20200034.
Mu, Z., Jiao, L., Wei, Q., Li, H., 2016. RSC Adv. 6 (49), 42994–42999.
Nguyen, A.H., Sim, S.J., 2015. Biosens. Bioelectron. 67, 443–449.
Nuzaihan, M.N.M., Hashim, U., Md Arshad, M.K., Kasjoo, S.R., Rahman, S.F., Ruslinda, A.R., Fathil, M.F., Adzhri, R., Shahimin, M.M., 2016. Biosens. Bioelectron. 83, 106–114.
Rahman, S.F., Yusof, N.A., Hashim, U., Hushiarian, R., M, N.M., Hamidon, M.N., Zawawi, R.M., Fathil, M.F., 2016. Anal. Chim. Acta 942, 74–85.
Sahoo, P., Suresh, Sumathi, Dhara, Sandip, Saini, Garima, Rangarajan, S., Tyagi, A.K., 2013. Biosens. Bioelectron. 44, 164–170.
Salimi, A., Kavosi, B., Fathi, F., Hallaj, R., 2013. Biosens. Bioelectron. 42, 439–446.
Shen, M.Y., Li, B.R., Li, Y.K., 2014. Biosens. Bioelectron. 60, 101–111.
Sun, S., Wang, R., Huang, Y., Xu, J., Yao, K., Liu, W., Cao, Y., Qian, K., 2019. Small 15 (34), 1902441.
Thiyagu, S., Devi, B.P., Pei, Z., 2011. Nano Research 4 (11), 1136–1143.
Tian, B.Z., Zheng, X.L., Kempa, T.J., Fang, Y., Yu, N.F., Yu, G.H., Huang, J.L., Lieber, C. M., 2007. Nature 449 (7164), 885–889.
Tsai, C.-C., Chiang, P.-L., Sun, C.-J., Lin, T.-W., Tsai, M.-H., Chang, Y.-C., Chen, Y.-T., 2011. Nanotechnology 22 (39), 135503.
Wan, J., Pei, C., Liu, C., Wang, Y., Cheng, D., Li, R., Shu, W., Zhang, C., Hu, W., Jin, J., Yang, Y., 2020. Angew. Chem. Int. Ed. 132 (27), 10923–10927.
Wang, Y., Springer, S., Zhang, M., McMahon, K.W., Kinde, I., Dobbyn, L., Ptak, J., Brem, H., Chaichana, K., Gallia, G.L., Gokaslan, Z.L., Groves, M.L., Jallo, G.I., Lim, M., Olivi, A., Quinones-Hinojosa, A., Rigamonti, D., Riggins, G.J., Sciubba, D. M., Weingart, J.D., Wolinsky, J.P., Ye, X., Oba-Shinjo, S.M., Marie, S.K., Holdhoff, M., Agrawal, N., Diaz Jr., L.A., Papadopoulos, N., Kinzler, K.W., Vogelstein, B., Bettegowda, C., 2015. Proc. Natl. Acad. Sci. U.S.A. 112 (11), 9704–9709.
Wu, C.-C., Manga, Y.B., Yang, M.-H., Chien, Z.-S., Lee, K.-S., 2018. J. Electrochem. Soc. 165 (13), B576–B581.
Yang, X., Fan, Y., Wu, Z., Liu, C., 2019. Micromachines 10 (11), 764.
Yang, X., Gao, A., Wang, Y., Li, T., 2018. Nano Research 11 (3), 1520–1529.
Yusoh, S.N., Yaacob, K.A., Alias, N.N., 2019. Mater. Res. Express 6 (11), 115005.
Zhang, H., Zhang, H.L., Aldalbahi, A., Zuo, X.L., Fan, C.H., Mi, X.Q., 2017. Biosens. Bioelectron. 89 (1), 96–106.
Zhang, N., Zhang, Z., Zhang, Q., Wei, Q., Zhang, J., Tang, S., Lv, C., Wang, Y., Zhao, H., Wei, F., Yan, J., Baklanov, M., Yin, H., Wang, W., Tu, H., 2020. Sensor. Actuator. B Chem. 306, 127464.
Zhang, R., Le, B., Xu, W., Guo, K., Sun, X., Su, H., Huang, L., Huang, J., Shen, T., Liao, T., Liang, Y., Zhang, J.X.J., Dai, H., Qian, K., 2019. Small Methods 3 (2), 1800474.
Zhang, W., Dai, Z., Liu, X., Yang, J., 2018. Biosens. Bioelectron. 105, 116–120.